Solar Physics
DOI: 10.1007/•••••-•••-•••-••••-•

Sunspot Rotation and the M-class Flare in Solar Active Region NOAA 11158

Alexander Li[1] · **Yang Liu**[2] ·

Abstract

In this paper, we measure the rotation of a sunspot in solar active region NOAA 11158 (Solar Target Identifier SOL2011-02-15) that was associated with an M-class flare. The flare occurred when the rotation rate of the sunspot reached its maximum. We further calculate the energy in the corona produced by the sunspot rotation. The energy accumulated in the corona before the flare reached $5.5\times\ 10^{32}$ erg, sufficient for energy requirements for a moderately big solar eruption. This suggests that sunspot rotation, which is often observed in solar active regions, is an effective mechanism for building up magnetic energy in the corona.

Keywords: Solar active regions · Solar flares · Sunspot rotation

1. Introduction

It is generally accepted that the released energy in flares and coronal mass ejections (CMEs) is from the magnetic field in the solar corona (*e.g.*, Forbes, 2000). Understanding how energy builds up and is stored in the corona and why the stored energy is released rapidly is the key to forecasting solar events. Two mechanisms are suggested to build up magnetic energy in the corona: magnetic flux emergence and surface flows. Magnetic energy in the corona comes from the twisted magnetic flux tubes emerging from the solar interior into the corona, and is generated by shearing and braiding the field lines by the surface motions on the solar surface (*e.g.*, Berger, 1984; Kusano *et al.*, 2002; Liu and Schuck, 2012). There are several surface motions observed in the Sun; among them is the rotation of the sunspots. The rotation braids field lines in sunspots, generating twist in sunspot's magnetic tubes that contain higher magnetic energy. Rotating sunspots are often observed in solar active regions (*e.g.*, Brown *et al.*, 2003). Intensive studies have been carried out to analyze properties of the rotating

[1] Saratoga High School, Saratoga, CA 95070, USA email: alexlioralexli@gmail.com
[2] W. W. Hansen Experimental Physics Laboratory, Stanford University, Stanford, CA94305-4085, USA email: yliu@sun.stanford.edu

sunspots (*e.g.*, Yan *et al.*, 2008; Zhu *et al.*, 2012; Komm *et al.*, 2012; Jain *et al.*, 2012), the relationship between rotating sunspots and solar eruptions (*e.g.*, Zhang *et al.*, 2008; Jiang *et al.*, 2012; Török *et al.*, 2013; Wang *et al.*, 2014), and the cause of sunspot rotation (Longcope and Welsch, 2000; Fan, 2009). However, a key question in understanding solar eruptions associated with rotating sunspots, the energy budget in the corona generated by the rotation of sunspots, is not well investigated. Does sunspot rotation generate sufficient energy for energy requirements in a moderately large solar eruption? Only a few studies have been conducted to address this question. Based on the Minimum-Current Corona (MCC) model (Longcope, 1996), Kazachenko *et al.* (2009, 2010) analyzed two active regions and reported that the energy produced by rotating sunspots is consistent with energy estimates from the observation of the subsequent flares. Their calculation is based on magnetic topology and its change during evolution. In this study, we will address this question using a different approach by calculating energy injection rate by sunspot rotation.

Solar active region (AR) NOAA 11158 is chosen for this study. This is an emerging active region, beginning to emerge on 12 February 2011 and finally developing into a complex, multipolar active region. This active region produced several major flares during its disk passage, including five M-class flares and one X-class flare, the first X-class flare in Solar Cycle 24. Because it is the first active region that has produced multiple major flares in Solar Cycle 24, a variety of research has been conducted to study sunspot formation (Toriumi *et al.*, 2014), emergence and evolution of the active region (*e.g.*, Liu and Schuck, 2012; Cheung and DeRosa, 2012; Jing *et al.*, 2012; Kazachenko *et al.*, 2014); energy buildup in the corona (*e.g.*, Sun *et al.*, 2012a; Liu and Schuck, 2012; Tziotziou *et al.*, 2013; Tarr *et al.*, 2013; Aschwanden *et al.*, 2014), instability of the magnetic field (e.g. Wang *et al.*, 2014; Liu *et al.*, 2013; Sun *et al.*, 2012b), solar eruptions (e.g. Wang *et al.*, 2012; Sun *et al.*, 2012a, 2012b; Inoue *et al.*, 2014; Yang *et al.*, 2014), and the impact of the eruption to the interplanetary space and the Earth (e.g. Huang *et al.*, 2014). There are several rotating sunspots in this active region. One sunspot associated with an X2.2 flare at 01:27 UT 15 February 2011 has been studied in detail (Jiang *et al.*, 2012; Wang *et al.*, 2014). In this study, we analyze another rotating sunspot and its association with an M2.2 flare at 17:26 UT 14 February 2011 in this active region.

The paper is organized as follows: Section 2 describes data used and the method for measuring rotation rate of the sunspot. Results are shown in Section 3. We conclude this study in Section 4.

2. Data and Methods

2.1. Data

The observational data used in this research are taken by the *Helioseismic and Magnetic Imager* (HMI; Scherrer *et al.*, 2012; Schou *et al.*, 2012) aboard *Solar Dynamics Observatory* (SDO; Pesnell *et al.*, 2012). The HMI instrument is a filtergraph covering full disk with 4096×4096 pixels. The spatial resolution is

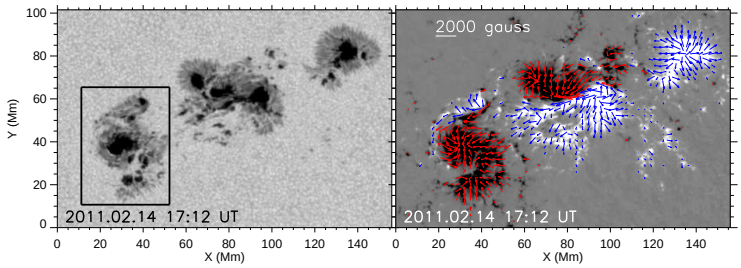

Figure 1. Intensity (left) and vector magnetic field (right) of AR 11158 at 17:12 UT on 14 February 2011. The rectangle in the left panel encloses the rapidly rotating sunspot of interest. The black-white image in the right panel represents the vertical magnetic field with positive polarity in white and negative in black. The image is saturated at ± 1000 gauss (G). The arrows refer to the horizontal field.

about 1" with a 0.5" pixel size. The width of the filter profiles is 76 mÅ. The spectral line used is Fe I 6173 Å which is formed in the photosphere (Norton *et al.*, 2006). The measurement is taken at six wavelength positions in the spectral line. The continuum intensity is obtained by reconstructing the spectral line profile from the measurements at the six positions (Couvidat *et al.*, 2012). The vector magnetic field is derived from the measurements of the linear and circular polarizations (Hoeksema *et al.*, 2014). The Stokes parameters (I, Q, U, V), determined by the polarizations, are inverted to retrieve the vector magnetic field using a Milne-Eddington (ME) based inversion algorithm, Very Fast Inversion of the Stokes Vector (VFISV; Borrero *et al.*, 2011; Centeno *et al.*, 2014). The 180° degree ambiguity of the azimuth is resolved using a "minimum energy" algorithm (Metcalf, 1994; Metcalf *et al.*, 2006; Leka *et al.*, 2009). The location and extent of the ARs are automatically identified and bounded by a feature recognition model (Turmon *et al.*, 2010), and the disambiguated vector magnetic field data of ARs are deprojected to heliographic coordinates (Bobra *et al.*, 2014). Here the Lambert (cylindrical equal area) projection method centered at the region is used for the remapping. The continuum intensity images are also mapped to heliographic coordinates using the same projection method. In this study, the continuum intensity and vector magnetic field data are used to analyze the rotating sunspot in AR 11158.

Figure 1 shows the continuum intensity continuum image (left) and the vector magnetic field (right) of this active region at 17:12 UT, 14 February 2011. The image in the right panel is the vertical magnetic field saturated at ± 1000 gauss (G), with the positive field in white and the negative in black. The horizontal field is represented with arrows. The rotating sunspot analyzed here is enclosed by the rectangle on the left panel; the horizontal field (right panel) shows an obvious rotation pattern, indicating field lines twisted around the sunspot.

The February 14 17:26 UT M2.2 flare took place in a newly emerged, small bipole just north of this rotating sunspot (Sun *et al.*, 2012b; Tarr *et al.*, 2013). The bipole exhibited quasi-counterclockwise motion along the rim of the rotating sunspot, showing a similar fashion of rotation. This may suggest a magnetic connection between the bipole and the pre-existing sunspot. Sun *et al.* (2012b) analyzed the topology of magnetic structure involved in this event, and suggested

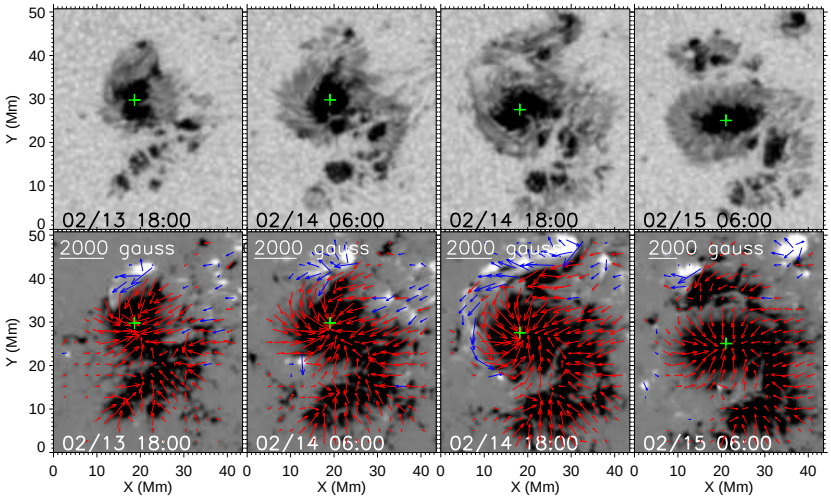

Figure 2. Evolution of the rotating sunspot: intensity (top) and vertical magnetic field (bottom). The sunspot grew and rotated rapidly in this time period. The images in the bottom panels, the vertical component of the magnetic field is saturated at ± 1000 G. The green pluses in the top panels represent the center of the rotating sunspot. These centers are also marked on the corresponding magnetograms, as shown in the bottom panels.

that a coronal null point, setting above the erupting flux tube, likely led to magnetic reconnection, triggering the eruption. A special field geometry guided this eruption propagating non-radially.

The evolution of the sunspot is shown in Figure 2. From the continuum intensity images in the top panels, one can clearly see that the sunspot rapidly rotated counter-clockwise until 06:00 UT, 15 February. The sunspot also has grown gradually with time. The vector magnetic field in the bottom panels shows an increase of magnetic twist that surrounded the sunspot, and this twist relaxed much later in time, as seen in the 06:00, 15 February data. The rotation rate of this sunspot is measured with the continuum intensity data that are described in detail in the following section.

2.2. Methods

The continuum intensity data from 13 to 17 February 2011 were used to measure the rotation rate of the aforementioned sunspot in AR 11158. The data cadence is 720 s. For each frame, a square shaped window of 75×75 pixels was cropped around the sunspot. For the first frame, the center of gravity (CoG) of the sunspot image was found, and its coordinates recorded. We measured the darkness (not brightness) of the sunspot to compute CoG. A threshold was set for the intensity so that the CoG calculation includes only the umbra and penumbra. A cross correlation method is then performed between the first frame and the second frame to find the shift between the two frames and align them (Fisher and Welsch, 2008). The aligned frames were mapped to a polar coordinate system with the CoG as the origin, where the X-axis in the mapped frames represents the polar angle around the origin and the Y-axis refers to the distance from the

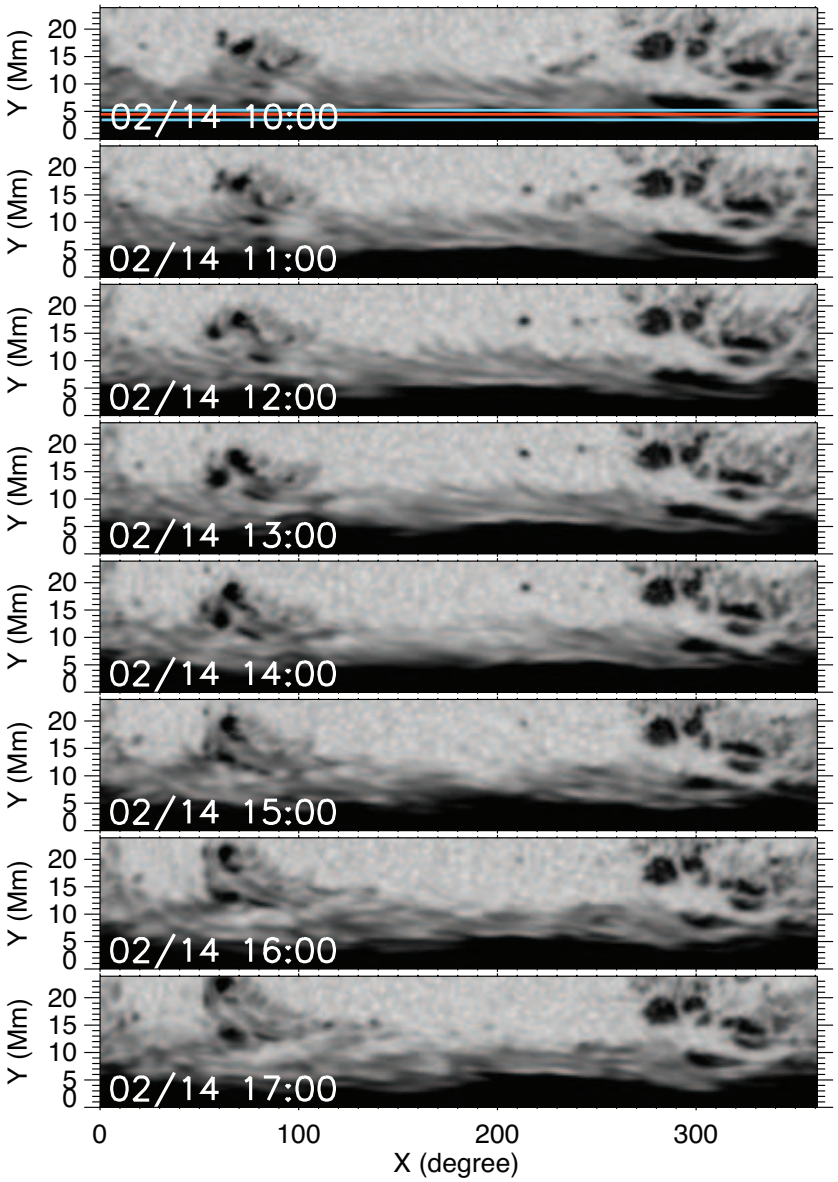

Figure 3. Stack of representative remapped intensity images of the rotating sunspot in polar coordinates. The X-axis refers to the angular coordinate in degrees; the Y-axis refers to the radial coordinate in Mm (in total 65 pixels). Time runs from top to bottom. The cross correlation technique is applied to the remapped images from 0 Mm – 4.35 Mm ($Y = 4.35$ Mm is denoted by the red line in the top panel) to derive the rotation angle in Method 1. The light blue lines ($Y = 3.63$ Mm and $Y = 5.07$ Mm) enclose an area used in Method 2 to determine the rotation rate.

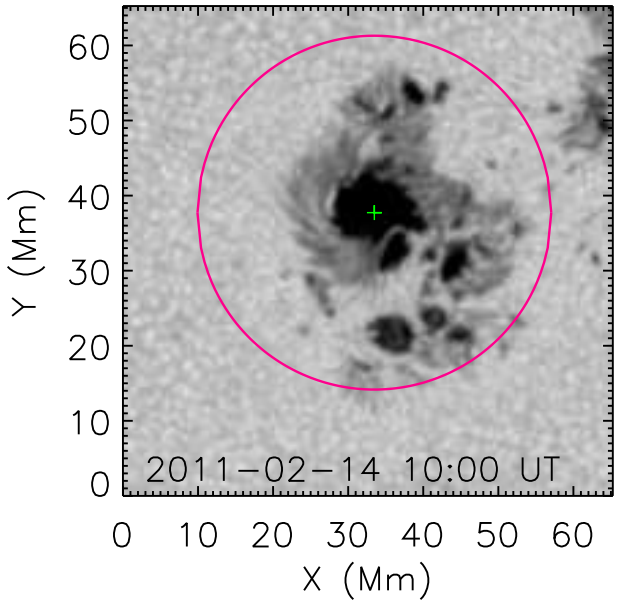

Figure 4. Intensity image of the rotating sunspot at 10:00 UT, 14 February 2011. Green plus denotes the CoG of the sunspot; pink circle encloses the area that is mapped to the polar coordinates as shown in the top panel of Figure 3.

origin, as shown in Figure 3. The pixel scale in the Y-axis (the distance from the origin) is 0.36 Mm, the same scale as in the original image at the disk center. The cross correlation was applied again to the mapped frames to derive the relative shifts of the two frames. The shift in the X-axis is the rotation angle of the sunspot within the time interval of the two frames. This procedure was repeated on the third as well as later frames. The derived rotation angle was divided by the time interval of two adjacent frames to obtain the rotation rate. Figure 3 shows examples of mapped frames of the sunspot at several representative times. The slice of each mapped frame used for performing the cross correlation has a range of 0°–360° in the X-axis and 0 – 12 pixels (roughly 0 Mm – 4.35 Mm, see Figure 3) in the Y-axis, as denoted by the red horizontal line (Y = 4.35 Mm) in the top panel of Figure 3. This approach is called *Method 1* hereafter. To provide another way to understand the remapped images, we show in Figure 4 an intensity image of the rotating sunspot taken at 10:00 UT on 14 February 2011. The green plus denotes the CoG of the image and the pink circle encloses the area that was mapped to polar coordinates, as shown in the top panel of Figure 3.

Another approach to measure the rotation of the sunspot is to trace representative features of the sunspot frame by frame. An effective way to trace features is to make a time-slice image of the features. This is the most common method used in previous papers (*e.g.* Brown *et al.*, 2003; Jiang *et al.*, 2012; Wang *et al.*, 2014). The method to generate the mapped frames in a polar coordinate system is the same as in Method 1. To avoid a shift of the features along the radial direction (Y-axis in the mapped frame), we calculated an average of five pixels

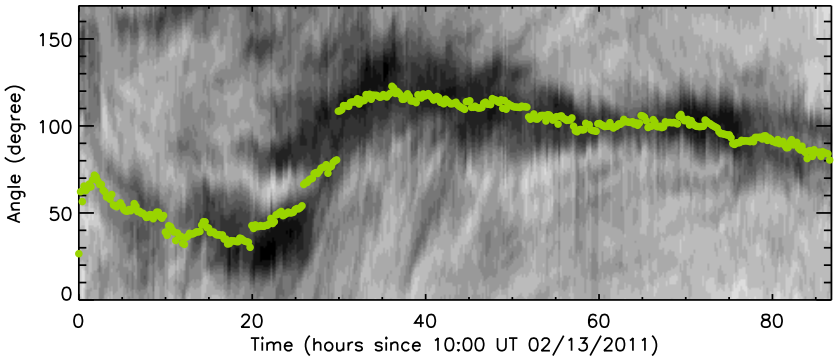

Figure 5. Time-slice taken from the remapped intensity images at a constant radius. Green dots denote locations of the tacked feature determined by measuring the CoG of each slice.

along the Y-axis, from 10th pixel to 14th pixel (from 3.63 Mm to 5.07 Mm, as marked by the light blue lines in the top panel in Figure 3). The selection of these five pixels ensures the inclusion of a representative feature that survived for a sufficiently long time. A stack with one average slice per frame forms the time-slice image, as shown in Figure 5. The CoG of each column in this time-slice image (green dots in the image) was derived, which corresponds to the center of the tracked feature. The rotation rate was determined from those identified locations using a linear fit to every 10 data points in time. This approach is called Method 2 hereafter. In Method 1, the cross correlation was applied to two frames that enclose the entire sunspot. The shift of the angle measured is deemed to be an average of the rotation for the entire sunspot. In other words, it represents a bodily rotation rate for the sunspot. Method 2, on the other hand, measures the rotation rate by tracing distinctive features. It requires that the features have a fairly long lifetime. It is not guaranteed that the measured features represent the sunspot as a whole, and the evolution and proper motion of the features add uncertainty to the measurement with Method 2.

Figure 6 exhibits a comparison of the rotation rates from the two methods. A 10-point running average was applied to the rate of Method 1 to match the 10-point linear fit in Method 2. The error bar in Method 1 is estimated by measuring the rotation rate from 11 different radius ranges. That is, we have chosen 11 slices of each mapped frame with Y-coordinate ranges of 0 – 11 pixels, 0 – 12 pixels, ..., and 0 – 21 pixels. We measured the rotation rates from those slices separately, and then obtained 11 measurements. The error reported in Figure 6 is the standard deviation of these 11 measurements. The error bar in Method 2 represents the error of the linear fit to 10 successive data points in time. Both methods have given a positive rotation rate (counter-clockwise) during most of the time and also captured the rapid spinning of the sunspot in the time period of 12:00 – 20:00 UT, 14 February 2011. This indicates that both methods are effective in measuring rotation for the time periods when the sunspots rotate significantly. In other time intervals, however, Method 2 measures the rotation rate as oscillating around the zero line, such as in the intervals of 20:00 UT, 13 February to 04:00 UT, 14 February and 22:00 UT, 14

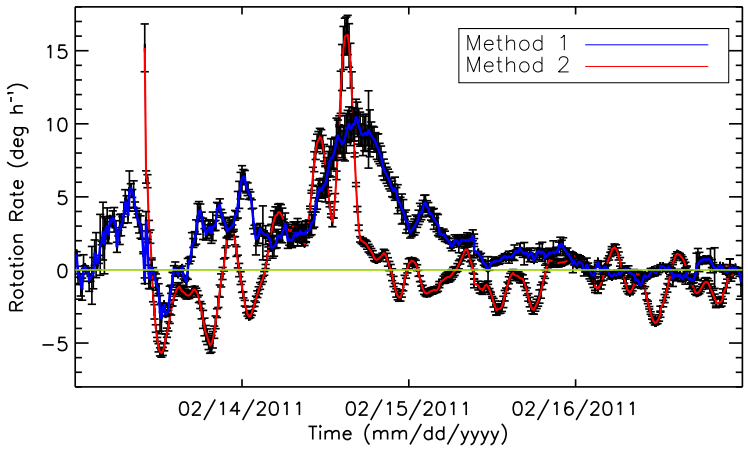

Figure 6. Rotation rates of the sunspot of interest measured from Method 1 (blue) and Method 2 (red) from 13-17 February 2011.

February to 12:00 UT, 15 February, when the sunspot obviously rotated counter-clockwise when viewed from a movie of the sunspot (The movie is available for viewing at $http://sun.stanford.edu/\sim yliu/sunspotrotation/$). It is worth noting that the measurements in Method 1 and Method 2 may have sampled for different portions of the sunspot. Method 1 basically measures the average rotation of the sunspot (or rigid rotation), whereas Method 2 measures the rotation of the specific feature traced. This is one limitation for Method 2 because the measured rotation may not represent the average rotation of the sunspot that we want to measure, and the chosen feature also needs to have a long lifetime in order to be traced during the entire procedure of interest. In this sense, it is not surprising that Method 1 performed better than Method 2. In the results shown in the next section, we have therefore adopted Method 1 to measure the rotation rate.

3. Results

The magnetic flux, rotation rate, vertical electric current, and energy flux in the rotating sunspot are analyzed in this study. The vertical electric current might be used as a proxy to estimate magnetic twist in the flux tube. Results are shown in Figure 7. From top to bottom are temporal profiles of magnetic flux, rotation rate, electric current, and energy flux (Poynting flux) across the photosphere (green curve, bottom panel), respectively, for the rotating sunspot observed in the period of 13-17 February 2011. The light blue curve in the bottom panel represents the accumulated energy in the corona that was computed by integrating the energy flux over time. The error bars in each panel refer to the standard deviation of the variables (1-σ). The red vertical lines denote the occurrence time of the M-class flare. The temporal profile of the magnetic flux

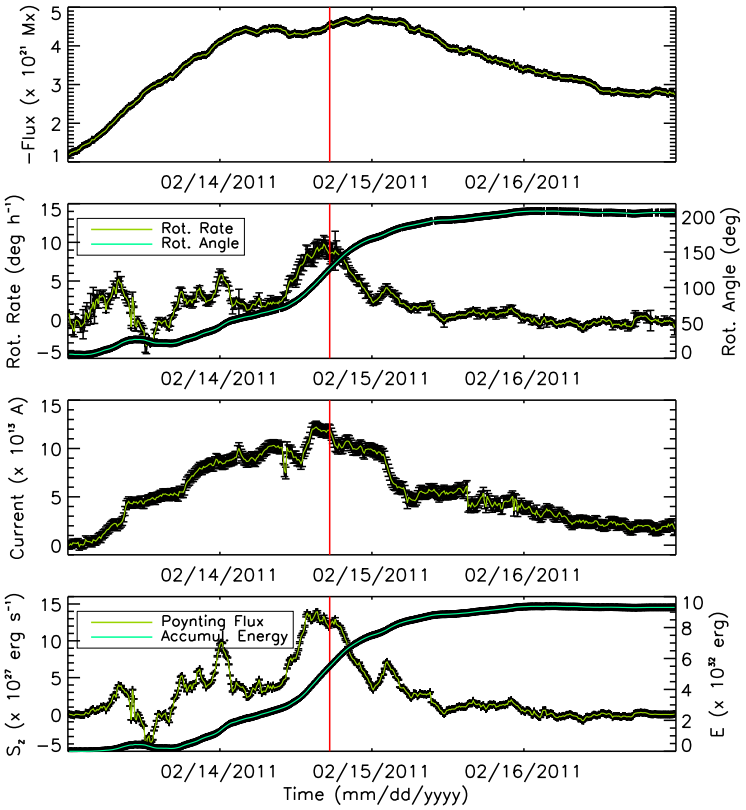

Figure 7. Temporal profiles of magnetic flux (top panel), rotation rate (green curve; second panel), electric current (third panel), and Poynting flux (energy flux across the photosphere) (green curve; bottom panel) for the rotating sunspot observed in the period of 13-17 February 2011. The magnetic flux was measured from only the negative field pixels with magnitude greater than 100 G. The light blue curve in the second panel represents rotation angle that was computed by integrating over time the rotation rate (green curve in the panel). The light blue curve in the bottom panel refers to the accumulated energy in the corona that was computed by integrating over time the Poynting flux. The red vertical line denotes the occurrence time of the M-class flare. The error bars in each panel represent one standard deviation (1-σ). For better visualization, the magnetic flux (top) that is negative, is multiplied by -1 here.

Φ (top panel) was computed by,

$$\Phi = \int_S B_z dS, \tag{1}$$

where B_z represents the vertical component of the magnetic field. Integration is done over the area that enclosed only the rotating sunspot. Only the negative field pixels whose magnitudes are greater than 100 G, 1-σ of the vertical magnetic field, were used in this integration. Thus the integral basically is the total flux of the rotating sunspot. It exhibits a monotonic increase from 00:00 UT, 13 February to 06:00 UT, 14 February, indicating the sunspot underwent quick emergence in this time period. The sunspot rotated rapidly in this time period (see the second panel). The rotation continued after the magnetic flux in this

rotating sunspot apparently stopped increasing, and reached its maximum just before the occurrence of the flare. The sunspot rotated through a total of 133° before the flare onset (light blue curve in the second panel).

It is often observed that the sunspots rotate when they emerge (*e.g.* Brown *et al.*, 2003). Longcope and Welsch (2000) proposed a dynamical model that suggests that only a fraction of the electric current carried by a twisted flux tube will pass into the corona. This leads to torsional Alfvén waves that propagate along the flux tube, transporting magnetic twist from the highly twisted portion of the flux tube under the photosphere to the less twisted portion of the flux tube that emerged and expanded in the corona. This process is manifested on the photosphere with rotational motions of sunspots. Pevtsov *et al.* (2003) tested this model with six emerging active regions. They found reasonable agreement between the model prediction and observation. MHD simulations successfully reproduced the processes the model predicted (*e.g.* Magara and Longcope, 2003; Fan, 2009). Thus, the rotation of the sunspot propagates magnetic twist into the corona and builds up free energy in the emerged magnetic field.

The electric current in the vertical direction I_z in area S is defined by

$$I_z = \int_S (\frac{\partial B_y}{\partial x} - \frac{\partial B_x}{\partial y}) dS, \tag{2}$$

where B_x and B_y are magnetic fields in the X- and Y-directions, respectively. The integration was carried out here over the area of interest. The vertical current in the rotating sunspot was calculated using vector magnetic field at the photosphere observed by HMI. As expected, the vertical current increased with time in the time period when the sunspot underwent emergence and quick spinning (see the third panel in Figure 7). It reached its maximum just before the occurrence of the flare and dropped dramatically afterwards. This implies that magnetic twist and energy quickly built up as the sunspot emerged and rotated, and relaxed after the eruption.

It is interesting to examine if the rotation alone could supply enough energy in the sunspot to explain the released energy in the flare. The energy flux, namely the Poynting flux $\mathbf{S}$, is $\mathbf{S} = c/4\pi \mathbf{E} \times \mathbf{B}$, where $\mathbf{E}$ is the electric field and $\mathbf{B}$ is the magnetic field. Consider pure rotation, and use cylindrical coordinates,

$$\mathbf{B} = B_r \hat{\mathbf{r}} + B_\theta \hat{\theta} + B_z \hat{\mathbf{z}}, \quad \mathbf{V} = V_\theta \hat{\theta}. \tag{3}$$

The electric field $\mathbf{E}$ is

$$c\mathbf{E} = -\mathbf{V} \times \mathbf{B} = V_\theta B_r \hat{\mathbf{z}} - V_\theta B_z \hat{\mathbf{r}}. \tag{4}$$

The Poynting flux in the vertical direction (the z direction), S_z, is then,

$$S_z = -\frac{1}{4\pi} V_\theta B_z B_\theta = -\frac{1}{4\pi} r\Omega B_z B_\theta, \tag{5}$$

where r is the distance between the pixel of interest and the rotation center, and Ω is the rotation rate.

Equation (5) was used to compute the energy flux across the photosphere purely due to the rotation of the sunspot. The vector magnetic field used is the observational data; the rotation rate was measured as described in the previous section. Results are presented in the bottom panel of Figure 7. The green curve represents the energy flux across the photosphere, while the light blue curve is the accumulated energy in the corona. The accumulated energy was computed by integrating over time the energy flux. It includes both the potential energy and free energy. It is clearly seen that the rotation continuously injected energy into the corona. The injection rate reached its maximum before the eruption of the flare. The energy built up purely by the rotation of the sunspot reached 5.5×10^{32} erg before the flare, sufficient for energy requirements for a moderately large flare/CME (Forbes, 2000). It suggests that, for this sunspot, rotation alone can supply the released energy needed for this M-class flare.

4. Conclusions and Discussion

The rotation rate of a sunspot in AR 11158 was measured using continuum intensity data taken by HMI. This rotating sunspot was associated with an M2.2 flare at 17:26 UT, 14 February 2011. It is found that the flare occurred when the rotation rate reached its maximum. The energy stored in the corona supplied from the rotation of the sunspot was further estimated. The energy estimated here includes both the potential-field energy and free energy. It reached 5.5×10^{32} erg, sufficient for energy requirements in a moderately large solar eruption. This suggests that rotating sunspots alone can be an effective mechanism for building up magnetic energy in the corona for solar eruptions.

This is one scenario of an energy source for this flare. As the flare took place in a newly emerged, small bipole, just north of this rotating sunspot (Sun *et al.*, 2012b; Tarr *et al.*, 2013), it is suggested that the bipole, undergoing strong shearing, built up non-potential magnetic energy that is thought to power this flare (Sun *et al.*, 2012b). Interestingly, the negative component of the bipole moved toward southeast, exhibiting quasi-counterclockwise motion along the rim of the rotating sunspot, and the positive component moved quasi-clockwise in a similar fashion. It is thus possible that the bipolar flux tube was somehow connected to the main sunspot beneath the surface. If so, the rotation rate may be related to the shearing motion of the flux tubes, and the energy injection rate (Poynting flux) at the bipole and the sunspot may be correlated as well. This connection deserves further investigation.

Acknowledgements The authors wish to thank the team members who have made great contributions to this SDO mission for their hard work. We are grateful to the anonymous referee for his/her comments and suggestions that improve the manuscript greatly. We thank M. Cheung at Lockheed Martin for helping derive the formula for energy flux calculation and G. Fisher and B. Welsch at UC Berkeley for providing the cross-correlation code. A. Li thanks the solar group at Stanford for offering this summer internship, through which he has begun to gain experience with research. The data have been used courtesy of NASA/SDO and the HMI science team.

References

Aschwanden, M. J., Sun, X., Liu, Y.: 2014, *Astrophys. J.* **785**, 34

Berger, M. A.: 1984, *Geophys. Astrophys. Fluid Dyn.* **30**, 79

Bobra, M. G., X. Sun, X., Hoeksema J. T., Turmon, M., Liu, Y., Hayashi, K., Barnes, G., Leka, K. D., 2014, *Solar Phys.* **289**, 3549

Borrero, J. H., Tomczyk, S., Kubo, M., Socas-Navarro, H., Schou, J., Couvidat, S., Bogart, R.: 2011, *Solar Phys.* **273**, 267

Brown, D. S., Nightingale, R. W., Alexander, D., Schrijver, C. J., Metcalf, T. R., Shine, R. A., Title, A. M. & Wolfson, C. J.: 2003, *Solar Phys.* **216**, 79

Centeno, R., Schou, J., Hayashi, K., Norton, A., Hoeksema, J. T., Liu, Y., Leka, K. D., Barnes, G.: 2014, *Solar Phys.* **289**, 3531

Cheung, M. C. M., DeRosa, M. L.: 2012, *Astrophys. J.* **757**, 147

Couvidat, S., Rajaguru, S. P., Wachter, R., Sankarasubramanian, K., Schou, J., Scherrer, P. H.: 2012, *Solar Phys.* **278**, 217

Fan, Y.: 2009, *Astrophys. J.* **697**, 1529

Fisher, G. H., Welsch, B. T.: 2008, In: Howe, R., Komm, R.W., Balasubramaniam, K.S., Petrie, G.J.D. (eds.), *Subsurface and Atmospheric Influences on Solar Activity*, *ASP Conf. Ser.* **383**, 373.

Forbes, T. G., 2000, *J. Geophys. Res.* **105**, 23153

Hoeksema, J. T., Liu, Y., Hayashi, K., Sun, X., Schou, J., Couvidat, S., *et al.*: 2013, *Solar Phys.* **289**, 3483

Huang, C., Yan, Y., Li, G., Deng, Y., Tan, B.: 2014, *Solar Phys.* **289**, 3109.

Inoue, S., Hayashi, K., Magara, T., Choe, G. S., Park, Y. D.: 2014, *Astrophys. J.* **788**, 182.

Jain, K., Komm, R. W., Gonzalez Hernandez, I., Tripathy, S. C., Hill, F.: 2012, *Solar Phys.* **279**, 349

Jiang, Y., Zheng, R., Yang, J., Hong, J., Yi, B., Yang, D.: 2012, *Astrophys. J.* **744**, 50

Jing, J., Park, S., Liu, C., Lee, J., Wiegelmann, T., Xu, Y., Deng, N., Wang, H.: 2014, *Astrophys. J. Lett.* **752**, L9

Kazachenko, M. D., Canfield, R., Longcope, D., Qiu, J.: 2009, *Astrophys. J.*, **704**, 1146

Kazachenko, M. D., Canfield, R., Longcope, D., Qiu, J.: 2010, *Astrophys. J.* **722**, 1539

Kazachenko, M. D., Fisher, G. H., Welsch, B. T.: 2014, *Astrophys. J.* **795**, 17

Komm, R., Howe, R., Hill, F.: 2012, *Solar Phys.* **277**, 205

Kusano, K., Maeshiro, T., Yokoyama, T., Sakurai, T.: 2002, *Astrophys. J.* **577**, 501

Leka, K. D., Barnes G., Crouch, A. D., Metcalf, T.R., Gary, G.A., Jing, J., Liu, Y.: 2009, *Solar Phys.* **260**, 83

Lemen, J. R., Title, A. M., Akin, D. J., Boerner, P.F., Chou, C., Drake, J.F., *et al.*: 2012, *Solar Phys.* **275**, 17

Liu, C., Deng, N., Lee, J., Wiegelmann, T., Moore, R. L., Wang, H.: 2013, *Astrophys. J. Lett.* **778**, L36

Liu, Y., Schuck, P. W.: 2012, *Astrophys. J.* **761**, 105

Longcope, D. W.: 1996, *Solar Phys.*, **169** 91

Longcope, D. W., Welsch, B. T.: 2000, *Astrophys. J.* **545**, 1089

Magara, T., Longcope, D. W.: 2003, *Astrophys. J.* **586**, 630

Metcalf, T. R.: 1994, *Solar Phys.* **155**, 235

Metcalf, T. R., Leka, K. D., Barnes, G., Lites, B.W., Georgoulis, M.K., Pevtsov, A.A., *et al.*: 2006, *Solar Phys.* **237**, 267

Norton, A. A., Pietarila Graham, J., Ulrich, R. K., Schou, J., Tomczyk, S., Liu, Y., *et al.*: 2006, *Solar Phys.* **239**, 69

Pesnell, W. D., Thompson, B. J., Chamberlin, P. C.: 2012, *Solar Phys.* **275**, 3

Pevtsov, A. A., Maleev, V. M., Longcope, D. W.: 2003, *Astrophys. J.* **593**, 1217

Scherrer, P. H., Schou, J., Bush, R. I., Kosovichev, A.G., Bogart, R.S., Hoeksema, J.T., *et al.*: 2012, *Solar Phys.* **275**, 207

Schou, J., Scherrer, P. H., Bush, R. I, Wachter, R., Couvidat, S., Rabello-Soares, M.C., *et al.*: 2012, *Solar Phys.* **275**, 229

Sun, X., Hoeksema, J. T., Liu, Y., Wiegelmann, T., Hayashi, K., Chen, Q., Thalmann, J., 2012a, *Astrophys. J.* **748**, 77

Sun, X., Hoeksema, J. T., Liu, Y., Chen, Q., Hayashi, K.: 2012b, *Astrophys. J.* **757**, 149

Tarr, L., Longcope, D., Millhouse, M.: 2013, *Astrophys. J.* **770**, 4

Toriumi, S., Iida, Y., Kusano, K., Bamba, Y.,Imada, S.: 2014, *Solar Phys.* **289**, 3351

Török, Temmer, M., Valori, G., Veronig, A. M., van Driel-Gesztelyi, L., Vrsnak, B.: 2013, *Solar Phys.* **286**, 453
Turmon, M., Jones, H. P., Malanushenko, O. V., Pap, J.M.: 2010, *Solar Phys.* **262**, 277
Tziotziou, K., Georgoulis, M. K., Liu, Y.: 2013, *Astrophys. J.*, **772**, 115
Wang, S., Liu, Wang, H.: 2012, *Astrophys. J.* **757**, L5
Wang, S., Liu, C., Deng, N., Wang, H.: 2014, *Astrophys. J. Lett.* **782**, L31
Yan, X. L., Qu, Z. Q., Kong, D. F., Xu, C. L.: 2012, *Astrophys. J.* 754, 16
Yan, X. L., Qu, Z. Q., Xu, C. L.: 2008, *Astrophys. J. Lett.* **682**, L65
Yang, Y., Chen, P. F., Hsieh, M., Wu, S. T., He, H., Tsai, T.: 2014, *Astrophys. J.* **786**, 72
Zhang, Y., Liu, J., Zhang, H.: 2008, *Solar Phys.* 247, 39
Zhu, C., Alexander, D., Tian, L.: 2012, *Solar Phys.* **278**, 121